Struct Bond (2016) 167: 81–106
DOI: 10.1007/430_2015_183

Published online: 9 October 2015

Realistic Simulation of Organometallic Reactivity in Solution by Means of First-Principles Molecular Dynamics

Pietro Vidossich, Agustí Lledós, and Gregori Ujaque

Abstract The application of first-principles molecular dynamics simulations to the study of the reactivity of organometallic complexes is surveyed, with special emphasis on studies addressing catalytic processes. We focused on modeling studies in which the solvent, either water or nonaqueous, is explicitly represented. Where available, comparison is made with results obtained from static calculations based on reduced model systems (clusters). In doing so, we show how the mechanistic insight provided by modeling studies of reactions involving charge separation (e.g., proton release) or unsaturated species may qualitatively and quantitatively change when more extended model systems are considered. General aspects of the methodology are also presented.

Keywords AIMD • Explicit solvent • Homogeneous catalysis • Organometallic reactivity • QM/MM-MD

Contents

P. Vidossich (✉), A. Lledós (✉), and G. Ujaque (✉)
Departament de Química, Edifici C.n., Universitat Autònoma de Barcelona, 08193 Cerdanyola del Vallès, Catalonia, Spain
e-mail: vido@klingon.uab.es; agusti@klingon.uab.es; gregori.ujaque@uab.cat

Abbreviations

AIMD	Ab initio molecular dynamics
CPMD	Car–Parrinello molecular dynamics
DFT	Density functional theory
MD	Molecular dynamics
QM/MM	Quantum mechanics/molecular mechanics

1 Introduction

Organometallic chemistry is possibly one of the fields in which the application of computational quantum chemistry methods has been most successful [1–3]. Indeed, it is now common practice to complement synthetic or spectroscopic studies with the computational characterization of putative species present in reaction mixtures [4–6]. Detailed mechanistic studies, employing state-of-the-art electronic structure methods (notably, density functional theory, DFT), may also be performed to rationalize experimental outcomes [7, 8]. Many of these studies are based on reduced model systems, in which the reactive moieties are represented explicitly and environmental effects are included by means of mean field theories [9–11]. The approach has turned out to be successful in many instances and may be routinely performed on general-purpose hardware.

But, is a continuum representation of solvent always sufficient? May we neglect specific solute–solvent interactions such as H-bonds? And what about reactions in which the solvent plays the role of a reactant? Furthermore, do species in solution interact, e.g., a charged catalyst with its counterion, and how would this affect the catalyst's reactivity? To address these and similar questions, we first have to extend the model systems considered to include an explicit representation of solvent and of those molecular species which may have an impact on reactivity. A first step in this direction is the use of cluster–continuum models in which a reduced number of explicit solvent molecules are introduced in the model. This approach has been successfully applied in computational studies of the organometallic reactivity [12–14], yet it suffers from some limitations [15]. How many solvent molecules should be explicitly included? Is the first solvation sphere enough? In order to mimic bulk conditions, models have to include enough solvent molecules to fully solvate the solute. These models, which are built to reproduce experimental densities, are generally treated as periodically repeating units in order to remove the explicit/continuum (or vacuum) boundary.

Dealing with large model systems however poses a challenge: how to explore its configurational space? Systematically investigating how the potential energy varies as a function of few nuclear coordinates, as is currently done in computational chemistry studies based on reduced model systems, is not viable because of the large number of particles involved. Statistical mechanics techniques, such as molecular dynamics or Monte Carlo, have to be used to sample the many configurations accessible by the system. The present review is an account of the use of molecular dynamics simulations to investigate organometallic reactions (see, e.g., [16] for an overview of the capabilities of first-principles MD simulations applied to chemical reactivity). A pioneering application of ab initio molecular dynamics (AIMD) simulations to the study of organometallic reactivity was published in the mid-1990s by Ziegler's group [17]. Because of the reasons outlined above, we focused on studies in which solvent was explicitly represented (see, e.g., [18] for an account of studies of organometallic systems in isolation). The material presented in this review is intended to highlight the relevance of including explicitly the solvent and what may be gained in doing so. We present selected mechanistic studies of several classes of reactions. It will become apparent to the reader that most studies investigated reactions performed in water. This certainly reflects the peculiar properties of water, including acid–base and coordinative properties. However, explicit modeling of other protic solvents (e.g., alcohols) and even apparently inert solvents such as toluene may be required to properly describe certain processes. We start with an accessible introduction of the methodology employed.

2 Methodological Aspects

Molecular dynamics (MD) is a simulation technique used to follow the time evolution of a molecular system [19, 20]. Within a classical representation of nuclei, the technique consists of solving numerically Newton's equations of motion [Eq. (1)] for all atoms in the system:

$$m_{\mathrm{I}} \frac{d^2 \boldsymbol{R}_{\mathrm{I}}}{dt^2} = \boldsymbol{F}_{\mathrm{I}}(\{\boldsymbol{R}_{\mathrm{I}}\}) = \; - \nabla_{\mathrm{I}} E(\{\boldsymbol{R}_{\mathrm{I}}\}) \qquad \mathrm{I} \; = \; 1 \cdots N \tag{1}$$

where m_{I} is the mass of atom I, $\boldsymbol{R}_{\mathrm{I}}$ its position vector, $\boldsymbol{F}_{\mathrm{I}}$ the force acting on it, and E the interaction potential function which depends on the positions of all the nuclei in the system. Several schemes have been proposed for a stable solution of Eq. (1), a popular one being Verlet's algorithm [21], which predicts the position at time $\boldsymbol{R}_{\mathrm{I}}(t + \Delta t)$ based on the position at time t and $t - \Delta t$ and the acceleration at time t:

$$\boldsymbol{R}_{\mathrm{I}}(t + \Delta t) = 2\boldsymbol{R}(t) - \boldsymbol{R}_{\mathrm{I}}(t - \Delta t) + \frac{\boldsymbol{F}_{\mathrm{I}}(t)}{m_{\mathrm{I}}} \Delta t^2 \tag{2}$$

The time step Δt used to solve Eq. (2) is a major parameter determining the stability of the simulation. For a proper propagation, Δt has to be chosen to be compatible with the highest vibrational modes of the system. When these involve bond stretching of hydrogen atoms, a time step up to 0.5 fs is appropriate. With a proper choice of Δt, solutions of Eq. (2) conserve the total energy of the system [19].

Simulations generally involve a fixed number of particles (N). To model bulk systems with a finite number of particles, periodic boundary conditions are applied. The volume (V) of the periodically repeating simulation box may be kept fixed or varied. Extensions to the scheme in Eq. (2) allow coupling the system to a thermostat and/or barostat to control the temperature T and pressure P of the system [22–24]. Hence, depending on the chosen conditions, the distribution sampled during the MD simulation is representative of either the microcanonical (NVE), canonical (NVT), or isothermal–isobaric (NPT) statistical mechanics ensembles [19].

Force evaluation is required for propagating nuclear positions [Eq. (2)]. This operation is repeated at each time step and has a major impact on the cost of the simulation. Forces are obtained as the gradients of some potential energy function E [Eq. (1)]. For large molecular systems, the so-called on-the-fly approach consists in calculating forces for each configuration $\boldsymbol{R}_\mathrm{I}$ visited by the system during the simulation. When forces are computed from first principles, the procedure is known as ab initio molecular dynamics (AIMD) [25]. Within the Born–Oppenheimer approximation, forces are computed after optimizing the wave function at each step during the dynamics (Born–Oppenheimer AIMD). To avoid this costly evaluation, Car and Parrinello developed an efficient and accurate scheme, according to which the orbitals are treated as classical particles and are propagated simultaneously with the ions [26].

Among the electronic structure methods to be used in AIMD simulations, density functional theory (DFT) [27], because of accuracy and favorable scaling with the number of atoms, is the recommended method to model organometallic systems. Extensive research has been dedicated to test and improve the performance of DFT when dealing with transition metal systems, and dedicated reviews cover recent developments [28–30].

According to the Kohn–Sham formulation of DFT [31], the energy of the system is given by Eq. 3

$$E = \min_{\{\varphi_\mathrm{i}\}} E_\mathrm{KS}\left[\{\varphi_\mathrm{i}(\boldsymbol{r})\}; \{\boldsymbol{R}_\mathrm{I}\}\right] + V_\mathrm{NN}(\{\boldsymbol{R}_\mathrm{I}\}) \tag{3}$$

where the E_KS functional contains kinetic, nuclear-electron, and electron–electron interaction energy terms, $\varphi_\mathrm{i}(\boldsymbol{r})$ are the molecular orbitals, and V_NN refers to the nuclear–nuclear interaction energy. The electron–electron term includes classical (Coulomb) and nonclassical interactions [32, 33]. The latter is accounted for by the exchange–correlation functional, E_xc, of which only approximate forms are known. Because of its approximate nature, E_xc is the main source of error in DFT calculations and thus of AIMD simulations. Some of the well-known deficiencies of E_xc

include the neglect of dispersion interactions, which are responsible for the underestimation of interaction energies between apolar fragments, and the so-called self-interaction error, which is responsible for the unphysical electron delocalization experienced in some open-shell systems [34]. Newly parameterized E_{xc} functionals [35], or the inclusion of empirical correction terms [36, 37], are capable of better describing van der Waals complexes. The inclusion of a fraction of exact (Hartree–Fock) exchange in the functional decreases the self-exchange interaction, improving the description of reaction barriers and open-shell systems [30]. However, in problematic cases, specific corrections have to be introduced as a remedy to the self-interaction error [38, 39]. DFT is a ground state theory, but extensions to treat excited states are available. Among these, time-dependent DFT (TD-DFT) found widespread application for the study of electronic transitions [40, 41].

Despite efforts to develop more efficient schemes (most notably, linear scaling methods) [42], the treatment of large systems by QM methods is computationally intensive (see [43, 44] for some notable examples of AIMD applications to systems of up to 1,000 atoms). To maintain the computational cost tractable, the multiscale quantum mechanical/molecular mechanical (QM/MM) approach may be used [45–47]. The approach, well established in the field of computational biochemistry [48, 49], consists in accurately modeling the chemistry at the reactive center (the organometallic frame, described at the QM level), while accounting for environmental (solvent) effects at the MM level. Since the original proposal, researchers have proposed different schemes to couple the QM and the MM subsystems (see, e.g., [48] for a comprehensive account). This approach has been extensively applied to modeling organometallic reactivity of systems with bulky substituents by means of traditional static methods, usually describing the reactive part at the QM level and the ligand and substrate substituents at the MM level [50–52]. Since then, developments to combine QM/MM potentials with ab initio molecular dynamics (QM/MM-MD) for the study of organometallic systems were described [53–57]. In the present context, the QM region may include solvent molecules if these are supposed to participate in the reaction. When these molecules are not strongly bound to the reactive moiety, diffusion may take place. To prevent exchange of QM and MM solvent molecules, either geometrical restraints have to be applied to the system [58] or sophisticated adaptive QM/MM partitioning schemes have to be adopted [59, 60].

Once the system is setup, the AIMD simulation is launched and extended for some amount of simulated time. As pointed out above, the system will visit states with a probability determined by the simulation conditions, e.g., Boltzmann statistics for a simulation performed at constant temperature. Accordingly, high-energy states, such as transition states, will be observed with low probability compared to the bottom of the free energy surface, which will be sampled more extensively. Because of the cost of AIMD simulations, the total accessible simulated time (of the order of hundreds of ps) is limited, and thus transitions (conformational transitions or chemical rearrangements) will likely not be observed during the simulation. A rough estimate of the simulated time required to observe a transition between two states separated by an energy barrier $\Delta G^{\ddagger}$ is $1/k^{TST}$, where k^{TST} is the transition state theory estimate of the rate constant [61]. To overcome this limitation,

enhanced sampling methods have been proposed [62]. Biased methods are particularly suitable to study chemical reactions, with thermodynamic integration [63] and metadynamics [64–66] being the ones that found widespread application in the field of AIMD. In both methods, one or few variables (hereafter, s), defined in terms of atomic positions, are used to drive the reaction. This set of variables is chosen as a representation of the reaction coordinate and thus is required to distinguish reactants from product (and intermediate) states. The bias acts to improve the sampling of these variables. In thermodynamic integration, a constraint is applied to maintain the reactive variable(s) at fixed values. The average force acting on the constraint in each constrained ensemble (the method is also known as constrained dynamics) [67, 68] is used to reconstruct the free energy of the process according to Eq. (4):

$$\Delta F(s) = -\int_0^s ds' \left\langle \frac{\partial H}{\partial s} \right\rangle_{s'} \tag{4}$$

In metadynamics, a history-dependent repulsive potential pushes the system away from stable states [69]. The potential is built along the dynamics as a sum of Gaussian functions which are added to the physical potential at intervals t':

$$V(s,t) = \sum_{t'} hexp\left[\frac{-(s(t) - s(t'))^2}{2w^2}\right] \tag{5}$$

where w is the width and h the height of the Gaussian functions. In the limit of $t \rightarrow \infty$, the (negative of) $V(s,t)$ approximates the underlying free energy. Guidelines on how to choose w and h may be found in [70, 71]. The convergence properties of $V(s,t)$ were studied in [72].

Because of the local nature of most chemical reactions, distances between reactive atoms are intuitive and appropriate choices for the s variables. It should be taken into account, however, that the cost of estimating free energy changes increases with the number of variables used to drive the reaction. Combination of variables may be an effective way to relieve this issue. For instance, in an S_N2 reaction, the difference of the distances of attacking and leaving group from the transferring group allows the use of a single variable to describe the process. A further issue to be taken into account is when the reactive species include chemically equivalent species as it occurs, for instance, in reactions in which water acts as the nucleophile. When bulk conditions are applied, any water molecule may attack the substrate. An appropriate s variable to take this into account is the coordination number (CN) [73]:

$$CN = \sum_i \frac{1 - (r_i/r_0)^p}{1 - (r_i/r_0)^q} \tag{6}$$

where r_i is the distance of the water oxygen atom i from the substrate atom and parameters p, q, and r_0 define the decay of the rational function.

It is important to note that the trajectories generated from biased simulations are not reactive trajectories. However, the biased simulation is interpreted in the sense that a reactive trajectory would pass through the same states visited in the biased simulation. Genuine reactive trajectories may be obtained launching simulations from high-energy configurations observed in the biased simulation [74].

Many popular quantum chemistry codes now include the possibility of performing AIMD simulations. Because of the need to propagate the equations of motion several thousands of times, highly efficient codes are required to perform AIMD simulations of complex molecular systems. The authors are more familiar with the CPMD (www.cpmd.org) and CP2K (www.cp2k.org) program packages, which were designed for atomistic simulations of large systems, and the applications presented in this review are mostly based on these codes. Both codes are particularly suited to high-performance computing resources but display good performances on general-purpose clusters provided with tightly coupled interprocess communications [75, 76]. Other codes implementing AIMD include VASP (www.vasp.at), GAUSSIAN (www.gaussian.com), deMon (www.demon-software.com), and Quantum ESPRESSO (www.quantum-espresso.org).

3 Applications

In this section, we illustrate applications of first-principles molecular dynamics simulations to the study of the reactivity of organometallic complexes in explicit solvent. We mostly focus on catalytic processes, although not always complete catalytic cycles have been addressed. We found convenient to distinguish reactivity in water (covered in Sect. 3.1) from nonaqueous solvents (covered in Sect. 3.2). This choice was made because of the prominent role of studies of aqueous systems in the field of first-principles simulations [77]. However, homogeneous catalytic processes are mostly developed in organic solvents, and the range of reactions experimentally studied is actually more diverse when we come to this class of solvents.

3.1 Reactivity in Water

Oxidation reactions in water are among the most studied processes by means of explicit solvent AIMD. In the Wacker, water splitting, and Shilov processes, proton release to the bulk solution is observed, a charge separation process which can be properly described in explicit solvent models. In the Fenton system, concerted radical propagation and proton transfer through the aqueous medium facilitate the formation of the high-valent iron catalysts. Cisplatin hydrolysis, a ligand exchange reaction, has been included as a prototype study addressing the coordinative properties of water, which are of high relevance for medicine-oriented design of

organometallic systems. The hydrogenation reaction promoted by ruthenium catalysts constitutes a clear example in which the presence of explicit solvent molecules stabilized charged intermediates. Further studies in which the effect of pH on the reactivity of transition metal systems is studied conclude this section.

3.1.1 The Fenton Chemistry

Fenton chemistry refers to an oxidation process that uses H_2O_2 as oxidant and a transition metal catalyst, generally Fe, to oxidize organic substrates. This process is commonly used for wastewater treatment. Two reaction mechanisms were proposed for the Fenton reagent. One assumes the production of free hydroxyl radicals by the metal-catalyzed decomposition of peroxide [78], whereas the other involves the formation of an iron–oxo complex, such as $[Fe^{IV}O(OH)(H_2O)_4]^{2+}$ (named hereafter $[Fe^{IV}O]^{2+}$), as a highly reactive oxidative intermediate [79].

Baerends and coworkers have largely contributed to the understanding of the Fenton process at the atomistic level. In a first contribution using explicit water AIMD simulations, they obtained important conclusions not affordable by means of static calculations [80]. They considered a cubic cell of ~10 Å edge including Fe^{2+}, H_2O_2, and 31 water molecules periodically repeating in space. The explicit representation of solvent allowed proper solvation of reacting species (Fe^{2+} and reaction intermediates) and, importantly, propagation of OH^-, H^+, and OH· through the solution.

Simulations established that the peroxide dissociates into two OH groups. One OH radical coordinates to the iron center. The other attacks a water molecule from the bulk rather than an iron-coordinated water molecule as suggested by calculations performed in gas phase. In a fast chain reaction, the OH· is passed on via two solvent water molecules, and the reaction is completed by abstraction of a hydrogen atom from an aqua ligand of the iron complex in the neighboring cell. The overall process was described as a concerted reaction rather than a chain reaction since the abstraction of a hydrogen atom from a coordinated aqua ligand occurred simultaneously with the breaking of the O–O bond. Formally, the overall process can be represented by

$$\left[Fe^{II}(H_2O)_5(H_2O_2)\right]^{2+} \rightarrow \left[Fe^{IV}(OH)_2(H_2O)_4\right]^{2+} + H_2O \qquad (7)$$

The Fe(IV) dihydroxide complex further evolved in solution to the formation of the $[Fe^{IV}O]^{2+}$ complex with the transfer of a proton to the bulk solution:

$$\left[Fe^{IV}(OH)_2(H_2O)_4\right]^{2+} + H_2O \rightarrow \left[Fe^{IV}O(OH)(H_2O)_4\right]^{+} + H_3O^+ \qquad (8)$$

Once again, the presence of explicit solvent was crucial to represent this pathway because it enabled an H^+ to be stabilized by the solvent molecules. In a subsequent study, the same group analyzed more deeply the formation of the $[Fe^{IV}O]^{2+}$

intermediate, corroborating that the process takes place in two steps and showing that from an energetic point of view, formation of the ferryl ion is more favorable than formation of free OH· radicals [81]. Recently, Yamamoto et al. [82] reinvestigated the mechanism of peroxide activation in $[Fe^{II}(H_2O_2)(H_2O)_5]^{2+}$ and confirmed the findings from the Baerends group.

The reactivity of the $[Fe^{IV}O]^{2+}$ species toward organic substrates was then investigated [83]. Using a model of similar size as the one used to model $[Fe^{IV}O]^{2+}$ formation, Baerends and coworkers performed constrained molecular dynamics simulations to estimate the energetics of two reaction mechanisms. One involved methane coordination, whereas the other, known as the oxygen-rebound mechanism (which is related to the proposed mechanism of methane oxidation by monooxygenase and cytochrome P450 enzymes) [84], implies an H abstraction to generate a CH_3· radical species, which then reacts with the iron complex to give the CH_3OH product. The two pathways were first evaluated by means of static methods. The mechanism based on methane coordination was found to be high in energy and was thus discarded by the authors. The rebound mechanism was modeled including the solvent explicitly. The free energy barrier for the H abstraction step was calculated to be 21.8 kcal mol^{-1}, much higher than in vacuum (3.4 kcal mol^{-1}). The spin density was mapped along the pathway to monitor to electronic state of the iron catalyst. Antiferromagnetic coupling between the reacting species was reported, with the iron complex in the high-spin $S = 5/2$ state.

The mechanism for methanol oxidation to formaldehyde by the $[Fe^{IV}O]^{2+}$ species was also investigated [85], as a prototype reaction for alcohol oxidation in Fenton chemistry. Two pathways were considered, with the $[Fe^{IV}O]^{2+}$ species attacking either the C–H bond or the O–H bond. Considerable differences in the energetics computed from gas phase and solution models were reported. The C–H bond pathway in the gas phase turned out to have a low barrier of 0.5 kcal mol^{-1}. In solution, however, the free energy barrier was estimated to have an upper bound of 12 kcal mol^{-1}. The subsequent step involving the O–H bond breaking proceeded spontaneously. The alternative pathway that involves coordination of MeOH and hydrogen transfer from the coordinated OH group could not be discarded because the energy barrier was found to be 10.5 ± 2.4 kcal mol^{-1}. The reactivity was proposed to be associated with the shape and energy of the LUMO of the $[Fe^{IV}O]^{2+}$ species (the Fe–O σ* orbital), suggesting that this species is a strong electron acceptor rather than an H-bond acceptor, thus facilitating the C–H bond activation of the organic compound. These ideas were recently further developed for the mechanism of C–H activation by $[EDTAH_n{\cdot}FeO]^{(n-2)}$ species [86].

3.1.2 The Wacker Oxidation

The Wacker process is a paradigmatic example of homogeneous catalysis applied in the chemical industry [87]. The process, discovered in the 1950s, produces acetaldehyde from ethene and oxygen using a Pd catalyst. The reaction is proposed to proceed via the addition of Pd and a hydroxide group (originated from the

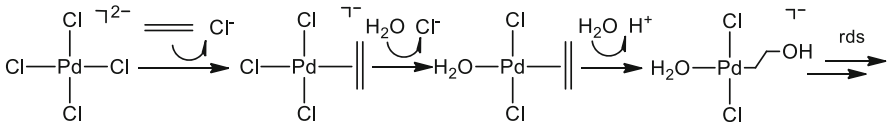

Fig. 1 Proposed sequence of steps for hydroxypalladation of ethene in the Wacker process

nucleophilic addition of a water molecule) across the C=C bond, a process named "hydroxypalladation" (Fig. 1) [88]. The mechanism of this step, crucial for the reaction, remained controversial over many years until recently [89].

A number of studies investigated the reaction mechanism by means of static methods [88, 89]. Many of these studies included a cluster of water molecules for a better modeling of the system, in particular of the proton transfer during the nucleophilic attack of a water molecule on the coordinated ethene. However, the use of an extended cluster of water molecules complicates the exploration of the potential energy surface due to the existence of several manifolds with similar energy. To overcome this limitation, free energy methods that account for finite temperature effects are required.

An important issue in the Wacker mechanism concerns the nature of the catalytically active Pd^{II} species. Ligand exchange at $[PdCl_4]^{2-}$ was studied by Kovács et al. [90] and Nair and coworkers [91, 92] by means of AIMD simulations in explicit water. Similar protocols were used, applying periodic boundary conditions to a cell of ~10 Å edge including the reactants and about 35 water molecules. The reactive events were explored by means of metadynamics.

The experimental rate law indicates that at low $[Cl^-]$, two Cl^- ligands are substituted by H_2O and C_2H_4. The *trans*-effect will determine the configuration of the $[PdCl_2(C_2H_4)(H_2O)]$ species. Calculations agree that the most likely pathway starts with the substitution of Cl^- by C_2H_4, followed by the exchange of a second Cl^- ligand for H_2O, generating *trans*-$[PdCl_2(C_2H_4)(H_2O)]$ (see Fig. 1). Remarkably, formation of the *trans* intermediate is of a considerable relevance for the reaction mechanism, because it implies the anti-nucleophilic addition by a water from the bulk (outer sphere mechanism), rather than the syn addition by a Pd-coordinated aqua ligand (inner sphere mechanism). Thus, explicit solvent simulations point to a more favored outer sphere mechanism. Importantly, the nucleophilic addition of water, leading to the formation of the C–O bond, takes place simultaneously to the proton release from the attacking water to the bulk solution.

The consequence of these observations is that the rate-determining step (rds) of the process should follow the hydroxypalladation to be in agreement with the experimental rate law. Bäckvall et al. [93] proposed a ligand dissociation step after the hydroxypalladation as the rds, although a β–hydrogen transfer, to form a Pd-hydride intermediate, has also been proposed [94] (although not supported by KIEs) [95]. The complete catalytic cycle was evaluated by means of metadynamics simulations for both forward and backward reactions (Fig. 2). The computed free energy profile showed that the rds involves *trans*-to-*cis* isomerization of Cl^- ligands and β–hydrogen elimination. The free energy barrier was associated with

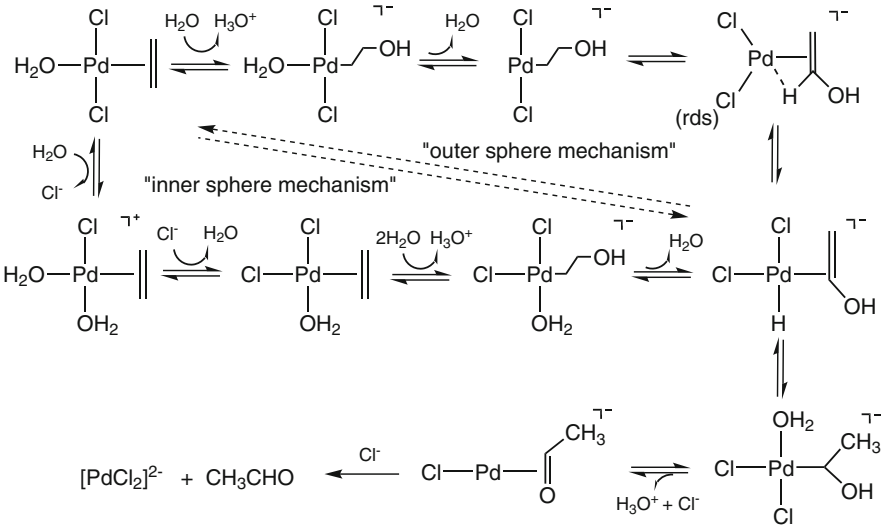

Fig. 2 Calculated reaction mechanisms for the Wacker process by AIMD simulations

the isomerization, because the formation of the Pd-hydride intermediate occurred immediately after as a barrierless process.

Another interesting part of the process concerns the formation of the aldehyde. This step involves the deprotonation of the OH group of the hydroxyethyl ligand. Several pathways were proposed in the literature for this step, including β–hydrogen elimination [96] and deprotonation by a Cl^- ligand [97] or by a water molecule from solution [91]. The three possibilities were accounted for in a metadynamics simulation, showing that the deprotonation occurs to a solvent water molecule (Fig. 2).

Interestingly, the free energy barriers of all the individual steps characterized during the simulation were used to build a kinetic model for the process. The experimental rate law could be reproduced using the values derived from first-principles molecular dynamics calculations [98].

3.1.3 Hydrolysis of Cisplatin

Cisplatin, *cis*-$[Pt(NH_3)_2Cl_2]$, is a compound of considerable relevance in medicine due to its application as an anticancer drug. The activity of cisplatin is due to coordination properties of the $Pt(NH_3)_2$ moiety, which is capable of binding DNA. Ligand exchange at the Pt center is thus an important aspect of drug activation. Cisplatin in aqueous environments exchanges Cl^- for aqua ligands (Fig. 3), and this reactivity was among the first applications of AIMD to investigate transition metal complexes.

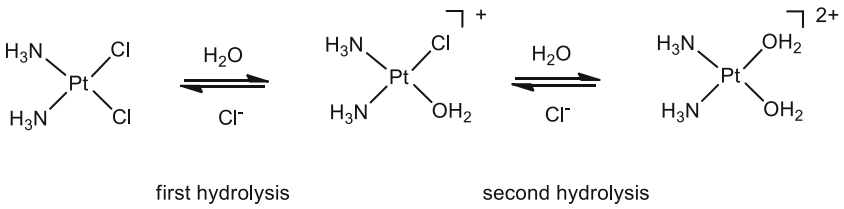

Fig. 3 Evaluated steps in the hydrolysis of cisplatin by CPMD calculations

Early studies using the Car–Parrinello approach were performed by Carloni et al. [99] The structure and dynamics of cisplatin in vacuum and water solution, as well as of the monoaqua complex, *cis*-$[Pt(NH_3)_2(H_2O)Cl]^+$, were analyzed. A periodically repeated cubic cell of 10.5 Å edge, including cisplatin and 35 water molecules, was considered. Importantly, the energies of the cisplatin and the monoaqua complexes were found to be the same within 1 kcal mol^{-1}. Hence, the presence of explicit water molecules, as a source of hydrogen bonds stabilizing the chloride ion, made the ligand substitution energetically accessible. In the gas phase, formation of the monoaqua complex would be highly endothermic because of the formation of separated charged species.

The free energy barrier for the chloride-by-aqua ligand substitution process was calculated via constrained molecular dynamics simulations at room temperature along an associative pathway. The estimated barrier of 21 kcal·mol^{-1} compared remarkably well with those obtained in several independent experiments, ranging from 23 to 26 kcal mol^{-1} ([100] and cites there in). The structure and dynamics of an adduct cisplatin–DNA was also investigated in water solution [99].

These studies were later extended by Lau and Ensing [101] by analyzing the two successive chloride-by-aqua ligand substitution process to form the *cis*-$[Pt(NH_3)_2(H_2O)_2]^{2+}$ complex from cisplatin. The ligand substitution processes were promoted by means of metadynamics, and umbrella sampling simulations were used to refine the free energy profiles. No assumptions on the nature of the mechanism (associative versus dissociative) were made in the choice of the variables used to drive the reaction. The free energy barriers obtained for the first and second chloride-by-aqua ligand substitutions were 23.3 and 18.5 kcal mol^{-1}, respectively; the relative free energies of the mono- and di-aqua complexes compared to cisplatin were 2.1 and −2.9 kcal mol^{-1}, respectively. The free energy estimates of both hydrolysis reactions of cisplatin were in very good agreement with experiments. Hydrolysis took place in a concerted manner, and tri- or penta-coordinated intermediates did not correspond to energy minima on the free energy profile. Interestingly, the dissociated Cl^- ion remained close (~4.5 Å) to the Pt complex, forming an ion-pair throughout the simulation. The hydration shell of cisplatin as well as of the mono- and di-aqua complexes have been studied by Sánchez-Marcos' group by means of classical MD simulations, but this study is out of the scope of this review [102].

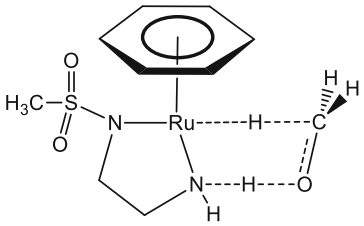

Fig. 4 The hydrogen transfer step studied by Pavlova and Meijer [101]

3.1.4 Ru-Catalyzed Hydrogen Transfer Process

The asymmetric hydrogenation of C=O and C=N bonds to generate stereogenic carbon centers is a transformation of great relevance for synthetic chemistry. The pioneering work of Noyori, who developed chiral Ru-based catalysts, was crucial in this field [103].

The key step of the process corresponds to the H_2 transfer from the Ru-based catalyst to the carbonyl group. Pavlova and Meijer studied this step by means of Car–Parrinello MD simulations using formaldehyde as the substrate, resulting in the formation of ethanol (Fig. 4) [104].

The authors used constrained dynamics to estimate the free energy barrier of the hydrogen transfer step. The reaction was studied in gas phase and water solvent. The calculated barrier for the hydrogenation of formaldehyde in water turned to be 3.4 kcal mol^{-1}, slightly lower than that obtained in gas phase, 5.3 kcal mol^{-1}. It was shown that when the hydride is transferred from the catalyst to the formaldehyde, the proton remains on the catalyst. The resulting methoxide intermediate was stabilized by multiple hydrogen bonds from surrounding water molecules. The proton transfer to the substrate was observed to take place from water molecules. Thus, explicit solvent simulations suggested a stepwise process, in agreement with kinetic isotope effect studies. Remarkably, this result is considerably different from that obtained in the gas phase, where the hydride and proton transfers were found to be concerted; recent studies combining cluster model with continuum methods (in alcohol as solvent) show a stepwise process (see Sect. 3.2.1).

The structural, energetic, and dynamical properties of bifunctional arene ruthenium catalysts have been investigated by means of classical and ab initio molecular dynamics simulations, although their reactivity was not addressed [105]. The hydrogen transfer reaction involving $NaBH_4$ hydrolysis has also been studied by means of explicit solvent AIMD [106].

3.1.5 Water Splitting Processes

The splitting of water into O_2 and H_2 is a major objective for the storage of solar energy into chemical fuels [107]. Two half-reactions are involved, namely, water oxidation, releasing O_2, H^+, and e^-, and reduction of protons to H_2. Water oxidation is a challenging process because of its multi-electron and multi-proton nature.

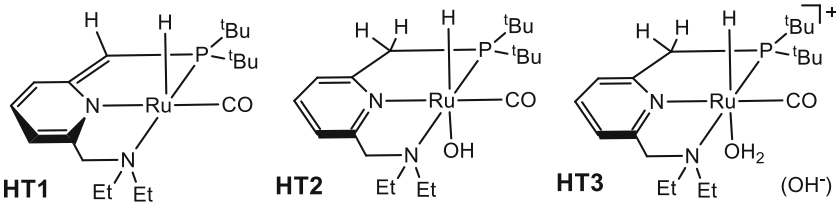

Fig. 5 Schematic representation of the Ru-pincer catalyst and the two pincer-aromatizated species proposed to form in solution on the basis of static and dynamic calculations

The discovery of Ru(II)-pincer complex as catalyst for this process demonstrated that a single metal center can promote the reaction [108]. Fabris and coworkers studied by means of AIMD calculations the reaction mechanism, illustrating the importance of describing the solvent explicitly [109]. Calculations were performed in a periodic cell (~13.5 Å edge) containing the catalyst and 73 water molecules. Reactive steps were promoted by means of metadynamics. Experimental measurements suggested that water addition to the Ru-pincer complex (HT1 in Fig. 5) yields HT2, featuring the aromatization of the pincer ligand by addition of a H^+ to the ligand and a hydroxo ligand to the metal. AIMD simulations based on the HT2 complex in explicit water showed that the hydroxo ligand spontaneously converted into an aqua ligand leaving a hydroxide in solution (HT3 in Fig. 5). Based on these results, the authors proposed an alternative route for the aromatization of the pincer ligand. Accordingly, the Ru-pincer complex coordinates a water ligand and takes an additional H^+ from a water molecule of the bulk solution. Based on simulations, the estimated activation free energy was found to be 8.8 kcal mol^{-1}.

H_2 formation was also investigated. H_2 forms from the addition of a proton to the Ru–H hydride. Two possible sources for the proton were considered: one in which the proton was coming from the pincer ligand (requiring a solvent water molecule to act as a proton shuttle) and the other in which the proton was coming from a solvent water molecule. The former route requires dearomatization–aromatization steps within the complete catalytic cycle. The latter route, which does not require the dearomatization–aromatization of the ligand, turned to be lower in energy, with a barrier of 20 kcal mol^{-1} (proton transfer from the ligand featured a barrier of 31 kcal mol^{-1}). These results allowed the authors to propose a new reaction mechanism where the Ru(II)-pincer always retains its aromatic character throughout the process.

The activity of other Ru-based catalysts for water oxidation has been investigated. Buda and coworkers addressed the reactivity of $[(Ar)Ru(X)(bpy)]^+$ (with X^- replaced by a water molecule) by means of AIMD calculations. The model system contained the catalyst and 73 water molecules in a periodic box of $16 \times 15.5 \times 15$ $Å^3$ [110]. The authors assumed a catalytic cycle in which the X^- ligand is initially replaced by a water molecule and the formed intermediate then undergoes two one-electron oxidation steps in which two protons are released leading to a ruthenium(IV)–oxo complex, $[(Ar)Ru(O)(bpy)]^{2+}$, with a strong radical character on the oxyl ligand. This species is supposed to be the active species in the

formation of the O–O bond with the nucleophilic attack of a water molecule onto the oxo ligand. This reaction step was the focus of the analysis by the authors. Two different reaction mechanisms were investigated for the formation of the O–O bond: one assuming that the incoming water molecule first binds to the Ru metal center and the other considering that the water molecule directly attacks to the oxyl ligand. Simulations show that water coordination to the oxo species was not viable because it leads to the breaking of the metal-aromatic ligand bond. The alternative pathway gives rise to the formation of the O–O bond generating a Ru-hydroperoxo complex; during this process, a proton is released to the water solution. The process was interpreted as a proton-coupled electron transfer on the basis of a charge distribution analysis. The aromatic ligand was suggested to play an important role as an electron charge buffer facilitating electron density adjustments during the catalytic cycle.

Buda's group also analyzed water oxidation as catalyzed by a di-Mn complex, $[(\text{bis(imino)pyridine})(H_2O)Mn^{IV}(\mu\text{-}O)_2Mn^{V}(O)(\text{bis(imino)pyridine})]^{3+}$ [111]. QM/MM-MD simulations were performed in a cubic box of 33 Å edge, containing the metal complex and around 1,000 water molecules. The di-Mn complex and three or four water molecules were included in the QM region, whereas the rest of the system was described at MM level. Full QM AIMD simulations were also performed in a periodic cell of $20.5 \times 23.8 \times 18.1$ Å^3, including 72 water molecules. Both setups consistently showed that the complex undergoes a structural rearrangement involving the release of the coordinated water molecule and the breakage of one of the oxo-bridges, thus generating two penta-coordinated Mn complexes bridged by an oxo ligand (Fig. 6a). Analysis of a subsequent reaction step for the O–O bond formation allowed the authors to conclude that both oxyl ligands at the Mn centers are involved in the process: one of them is attacked by a water molecule leading to the formation of a hydroperoxo ligand, whereas the other accepts a proton from the attacking water, thereby keeping the total charge of the complex unchanged (Fig. 6b).

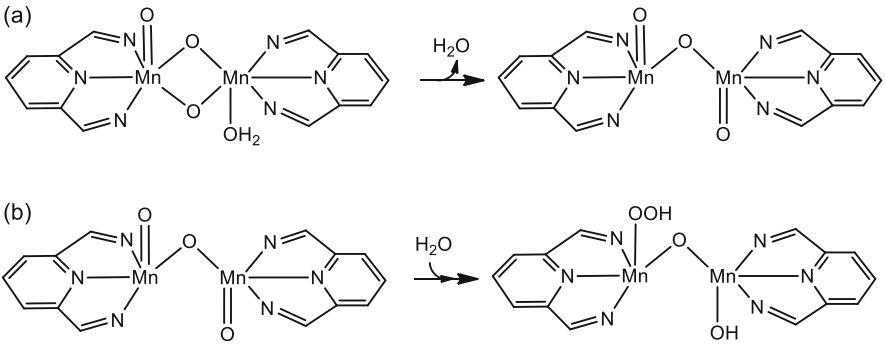

Fig. 6 (**a**) Rearrangement of the di-Mn structure in the solvent environment. (**b**) Reaction step for the O–O bond formation between the di-Mn complex and a water molecule [111]

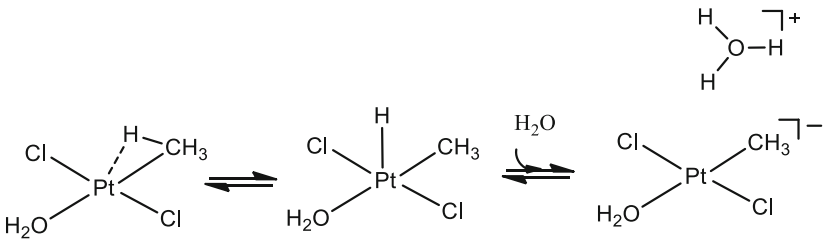

Fig. 7 Methane C–H bond activation by Pt^{II}

3.1.6 The Shilov Reaction

Alkane functionalization is a highly desirable chemical transformation. The Shilov system [112], based on Pt^{II} and Pt^{IV} complexes, constitutes an early proposal for hydrocarbon oxidation in aqueous solution (Fig. 7). The rate-limiting step of the catalytic cycle, namely, C–H bond activation, was investigated by Vidossich et al. by means of Car–Parrinello molecular dynamics simulations in explicit water [113]. The authors considered the $PtCl_2(H_2O)(CH_4)$ species, in both *cis* and *trans* configurations, solvated with 32 water molecules in a cubic box of ~10 Å edge treated under periodic boundary conditions.

The *trans*-$PtCl_2(H_2O)(CH_4)$ species turned not to be stable and spontaneously evolved to the methyl complex in the early stages of the simulation. Initially, the oxidative addition of the C–H bond to the Pt center resulted in a square pyramidal complex. Subsequently, the apical proton was released to a water molecule of the hydration sphere, resulting in the formation of a square planar methyl complex. On the contrary, the *cis* complex was maintained during the timespan of the simulation. The breakage of the C–H bond was thus promoted via metadynamics and required 6.4 kcal mol^{-1} free energy of activation. Similarly to the *trans* isomer, the proton moved to the Pt center to form a square pyramidal Pt complex, which spontaneously evolved to the square planar methyl complex by the release of the proton to the bulk solution. The activation barriers of the *cis* and *trans* σ-complexes were in line with previous work based on static calculations, and their difference was rationalized in terms of the effect of the ligand *trans* to methane. However, the high acidity of the five-coordinated hydride intermediate resulting from C–H activation could be revealed only by the use of explicit solvent models. Remarkably, the simulations showed that release of a proton to the hydration sphere was faster than water coordination to stabilize the formally Pt^{IV} center.

3.1.7 Other Processes

This subsection covers other important processes related to the reactivity or behavior of transition metal complexes in water solvent.

Reductive dehalogenation of chloroalkenes is an important process within the context of detoxification of halogenated pollutants. Bühl and Golubnychiy [114]

analyzed the evolution of a relevant intermediate generated in a Co-catalyzed dehalogenation process. Coordination of $Cl_2C{=}CCl_2$ to $[Co(glyoximato)_2]^-$ may proceed either via the release of a chloride and the formation of a vinyl complex or via the protonation of the chloroalkene ligand thus avoiding the formation of the vinyl complex. CPMD simulations were performed in explicit water to provide a microscopic description of the solvent, which is an important aspect for accurate computations of acidity constants. Calculations were performed under periodic boundary conditions using a cubic cell of ~13 Å edge containing the cobalt complex and 57 water molecules. Free energies were obtained by thermodynamic integration. The free energy for the protonation step turned out to be 10 kcal mol^{-1}, much smaller than that estimated from static calculations (30 kcal mol^{-1}). Importantly, AIMD calculations showed that the protonation process is not only thermodynamically favored but also kinetically over the formation of the vinyl complex.

Bühl and coworkers characterized the behavior of the uranyl ion (UO_2^{2+}) in water solution by means of first-principles molecular dynamics [115]. In a first study, water exchange at the hydrated uranyl was investigated. Both the dissociative and associative pathways were evaluated. The associative pathway turned to be the favored one by ~ 4 kcal mol^{-1}, in line with static results but somewhat underestimated compared to experiment [116]. The exchange between the terminal oxo atom and an O atom from bulk water in uranyl hydroxide complexes in basic solution $[UO_2(OH)_4]^{2-}$ was also investigated [117]. Simulations showed that the $[UO_3(OH)_3]^{3-}$ intermediate is obtained via deprotonation of the starting complex. The rate-limiting step turned to be the proton transfer from the hydroxo to the oxo ligand, a process assisted by a solvent water molecule. The overall barrier of 12.5 kcal mol^{-1} was in reasonable agreement with calculated value of 15.2 kcal mol^{-1} obtained from a static model [118], and the agreement is further improved compared to experiments [119].

The hydration/dehydration equilibria of a hydrogentungstate anion, $[WO_3(OH)]^-$; tungstic acid, $[WO_2(OH)_2]$; and protonated tungstic acid, $[WO_2(OH)(H_2O)]^+$ were studied by means of AIMD calculations in a cubic cell box of ~10 Å edge including the metallic species and 29 water molecules by Rodríguez-Fortea, Poblet, and coworkers [120]. The authors showed that increased acidity (decrease of pH) resulted in an expansion of the coordination sphere of the W^{VI}. At the simulated conditions, the tungstic acid did not protonate. Results were not in agreement with continuum methods.

Polyoxometalates (POMs) comprise a class of polynuclear metal–oxygen clusters usually formed by Mo, W, and V and sometimes other metals. With the ambitious and long-term objective of understanding the nucleation mechanism in the formation of the Lindqvist anion $[W_6O_{19}]_{12}^-$, Rodríguez-Fortea, Poblet, and coworkers have investigated dinuclear and trinuclear intermediates that were observed in ESI-MS experiments [121]. Calculations were performed in a periodic cubic box of ~12.6 Å edge including the metal intermediate and about 60 water molecules, depending on the metallic species. The authors observed that the coordination sphere of W^{VI} ions can expand by binding water molecules from the

bulk solution. Carbó and coworkers have investigated the behavior of selected Zr-monosubstituted monomeric and dimeric POMs in water solvent at different pHs [122]. Calculations suggested that the Zr metallic centers have a flexible coordination environment, with the tendency to reach coordination numbers greater than six (binding up to three water molecules).

The behavior of other transition metal complexes and ions in aqueous solution has been also investigated. For instance, the solvation of $[Ru(bpy)_3]^{2+}$ in water was evaluated by means of QM/MM-MD calculations in the ground [123] and the triplet excited state [124]. A similar study concerned the $[Fe(bpy)_3]^{2+}$ complex [125]. With the purpose of improving the accuracy of computed Pt NMR chemical shifts, the hydration properties of a set of negatively charged Pt complex ions ($[Pt(X_n)]^{2-}$; X=Cl, Br, and CN) were analyzed by means of AIMD calculations [126]. Hydration studies of square planar Pd^{II}- and Pt^{II}-hydrated complexes revealed interesting behavior in the non-equatorial region, with Pd and Pt behaving differently with respect to the interaction with solvent water molecules [127, 128]. AIMD simulations of *trans*-$PtCl_2(NH_3)$(Nglycine) in explicit water supported the formation of Pt···HO H-bond interactions between Pt and water molecules in solution [129].

3.2 *Reactivity in Nonaqueous Solvents*

The application of first-principles molecular dynamics to the study of organometallic systems or homogeneous catalytic processes in nonaqueous solvents is certainly less extended than in water. Nevertheless, a survey of the literature shows that the number of AIMD-based studies in nonaqueous solvents is increasing. In many cases, due to the larger size of the complexes investigated and of the solvent molecules compared to in-water studies, the hybrid QM/MM approach is taken to simulate realistic model systems at a reduced computational cost. Simulations by means of first-principles molecular dynamics on ionic liquids [130] or frustrated Lewis pairs in organic solvents [131] are not covered here.

3.2.1 Ru-Catalyzed Hydrogen Transfer in Methanol

As commented in Sect. 3.1.4, the asymmetric hydrogenation of C=O and C=N bonds is a fundamental transformation in chemistry for the generation of stereogenic centers. Noyori developed Ru-based chiral catalysts [103], whose reaction mechanism has been extensively investigated [132].

Handgraaf and Meijer investigated the reaction mechanism when methanol is the solvent by means of AIMD simulations [133]. Calculations were performed on a model catalyst, $[Ru(C_6H_6)(OCH_2CH_2NH)]$, including 40 molecules of MeOH in a periodic cubic box of ~14 Å edge. Constrained dynamics simulations were performed to estimate the free energy associated with the reaction steps. During

the process, a proton and a hydride (H^+, H^-) are formally transferred from methanol to the catalyst in an outer sphere mechanism, i.e., the substrate does not coordinate to the metal. The free energy profile of the process in solution showed a plateau zone associated with the proton transfer from the OH group of the substrate to the N of the amide ligand. This proton transfer results in a terminal oxygen with three lone pairs that was described as a methoxide-like species stabilized by hydrogen bonds from solvent (MeOH) molecules. Calculations performed in gas phase showed that at the transition state, the proton is moving from oxygen (MeOH) to the nitrogen ligand but is not yet fully transferred; on the contrary, in solution, the transfer is complete. Then, the intermediate evolves by transferring the second hydrogen to Ru (formally as H^-), thus converting the methoxide transient species in formaldehyde.

The reverse reaction, i.e., the reduction of formaldehyde to yield methanol, was also studied. It was observed that the hydride moves from Ru to formaldehyde, yielding the methoxide-like species. Such species made a strong hydrogen bond with a MeOH solvent molecule that was also interacting with the N of the amide ligand. Then, a proton transfer from this MeOH solvent molecule to the methoxide-like species took place, converting the former in a methoxide-like species and the latter in methanol. Subsequently, a second solvent molecule donated a proton to the newly formed methoxide molecule. Hence, a chain of proton transfer events was revealed to take place during the process. The simulation was extended to show that eventually the solvent-stabilized methoxide molecule finally exchanges a proton with the Ru complex to form the dehydrogenated Ru complex and methanol.

3.2.2 Ligand Substitution in Pd^0 Complexes in Toluene

Palladium/phosphine systems are among the most used catalytic systems in organic synthesis, as recognized by the assignment of the 2010 Nobel Prize in Chemistry (www.nobelprize.org/nobel_prizes/chemistry/laureates/2010). A debated issue in this field concerns the identification of the catalytically active species, which is crucial for understanding the reactivity of the system. Knowledge of which species are present in solution is a very important step toward this understanding. Pd^0 complex is generated in solution by ligand loss or exchange and may involve participation of solvent molecules. Low coordinated Pd–phosphine complexes are supposed to be more reactive. Pd(phosphine)$_2$ could actually be isolated, whereas the monophosphine species, Pd(phosphine), could not be characterized. Vidossich et al. [134] have used QM/MM-MD simulations to study the speciation of the Pd–phosphine system in explicit toluene. Several ligand exchange processes were evaluated in a periodically repeating box containing Pd^0, tri-phenyl phosphine (s) (PPh_3), and around 1,000 toluene molecules.

The behavior of Pd(PPh_3) in toluene was addressed by running QM/MM-MD simulations including the metal complex and four toluene molecules in the QM part. A toluene molecule was observed to coordinate to the metal center at the very beginning of the simulation and maintained the coordination to the metal center for the rest of the simulation. Actually, a second toluene molecule was observed to

coordinate to the metal center forming [Pd(PPh_3)($Tol)_2$]. However, the lifetime of this species was limited to few ps. Thus, the monophosphine Pd species is not accessible in toluene, a solvent generally considered as non-coordinating. The species with a single coordinate toluene appears as the most favorable one, but a second solvent molecule may bind the metal center, at least transitorily.

The behavior of $Pd(PPh_3)_2$ in toluene solution was also evaluated. Simulation showed a toluene molecule moving in and out the coordination sphere of Pd during the simulation. Accordingly, the free energy barrier of this process, computed by means of umbrella sampling simulations, was found to be small (2.4 ± 0.5 kcal mol^{-1}), with the tricoordinated species lying 1.8 ± 0.6 kcal mol^{-1} higher in energy than the $Pd(PPh_3)_2$ complex. The free energy associated with PPh_3 dissociation process from the [$Pd(PPh_3)_2$(Tol)] complex was estimated to be 17.3 ± 0.6 kcal mol^{-1}. This set of simulations provided evidence for the formation of several solvent adducts such as [$Pd(PPh_3)_2$(Tol)], [Pd(PPh_3)(Tol)] and [Pd(PPh_3)($Tol)_2$], whereas the bare [Pd(PPh_3)] species showed a too limited lifetime to be accessible in solution.

3.2.3 Dynamic Behavior of Agostic Interactions

Agostic interactions are intramolecular interactions between a C–H bond of a ligand and an electron-deficient metal center. These interactions are commonly observed to occupy a vacant coordination site in transition metal complexes, which would otherwise be coordinatively unsaturated. Agostic interactions may be seen as the first stage of C–H bond activation processes. The dynamic behavior of agostic complexes was investigated by QM/MM-MD simulations by Ortuño et al. [135]. The objective of this study was to reveal whether the C–H is kept firmly bonded to the metal center or rather fluxionality among equivalent C–H bonds would take place. The authors selected a set of three-coordinated T-shaped Pt^{II} complexes showing diverse agostic geometries. In the three Pt^{II} complexes considered, agostic interactions may involve C–H bonds at β (complex Pt_1), δ (complex Pt_2), and ζ positions (complex Pt_3, Fig. 8). The organometallic complexes were described at the quantum mechanical level, whereas the ~ 1,000 dichloromethane solvent molecules and the $[SbF_6]^-$ counterion were described by means of molecular mechanics. Simulations were run for 15 ps for each of the complexes at 300 K. The results show quite different behavior in solution for each complex.

In complex Pt_1 the agostic interaction is maintained throughout the simulation. The average Pt···C and Pt···H distances were comparable to those obtained from geometry optimization. Simulation of complex Pt_2 showed that the methyl groups of the *tert*-butyl substituent interchanged interaction with the metal center, providing an atomistic picture on how the averaging of the NMR signals of the three methyl groups takes place. Simulation of complex Pt_3, in which the C–H bond involved in the agostic interaction is six bonds away from the metal center, showed an easy rotation of the CH_3 groups of the isopropyl substituent. It was also observed that for short time intervals (few ps), the agostic interaction may break. Thus, these

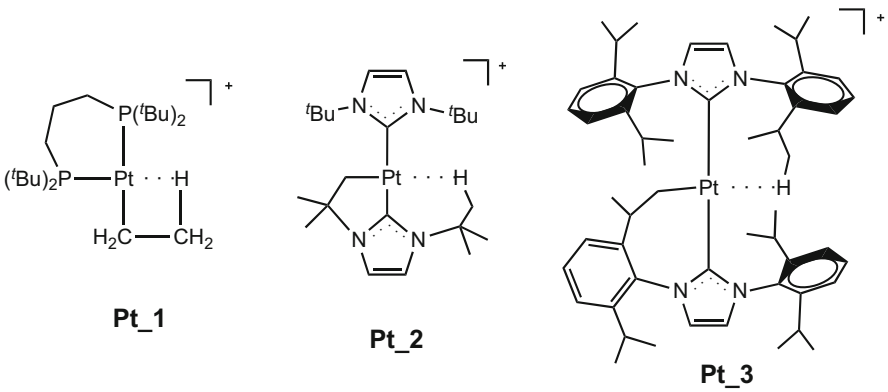

Fig. 8 Schematic representation of the three Pt^{II} complexes featuring agostic interactions studied by Ortuño et al

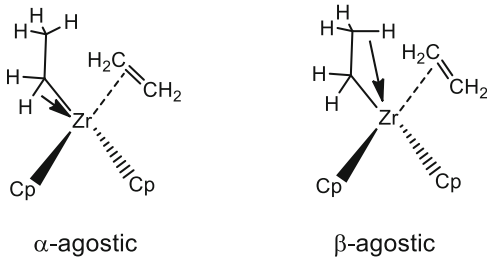

Fig. 9 Schematic representation of α- and β-agostic zirconocene complexes studied by Rowley and Woo [135]

set of simulations were able to reveal a range of dynamical behaviors of Pt···H–C agostic interactions.

Group IV metallocene catalysts are of major importance in olefin polymerization chemistry. Rowley and Woo [136] studied the dynamic behavior of agostic interactions in an archetypal zirconocene–olefin complex, $[(Cp)_2Zr(C_2H_5)(C_2H_4)]^+$. The authors were interested in exploring how the counterion, $[CH_3B(C_6F_5)_3]^-$, affects the reactivity of the complex. More specifically, the counterion effect on the relative stability and the free energy barrier for the interconversion process between the α- and β-agostic interactions were addressed (Fig. 9). Molecular dynamics is indeed an appropriate approach to the modeling of ion pairs in solution. QM/MM-MD simulations were performed at 300 K in explicit pentane solvent. The metallocene was described at QM level, whereas the counterion and the solvent molecules were represented at the MM level. The interconversion process between the α- and β-agostic complexes was studied in the presence and absence of the counterion. Interestingly, simulations of the complex in the presence of the counterion showed spontaneous isomerization from the β-agostic to the α-agostic configuration. Conversely, static calculations predict the former to be more stable by

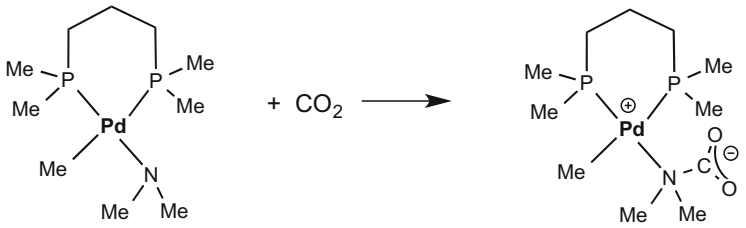

Fig. 10 Reaction step studied for CO_2 activation by a Pd complex in CO_2 under supercritical conditions

2.7 kcal mol^{-1}. The free energy profile of this process was calculated using umbrella sampling simulations. The barrier was found to be 2.8 kcal mol^{-1}, with the β-agostic species 1.6 kcal mol^{-1} lower in energy. Calculations including the counterion resulted in a barrier of 1.9 kcal mol^{-1}, with the β-agostic species 1.0 kcal mol^{-1} more stable than the α-agostic species. The authors attributed the stabilization in the presence of the counterion to the more favorable dipole–counteranion interaction in the more polar α-agostic configuration.

3.2.4 Addition of CO_2 to a Pd Complex in CO_2

Growing interest is shown toward catalysts capable of activating small molecules such as carbon dioxide [137]. Kirchner and coworkers [138] studied the addition of carbon dioxide to a Pd complex with an amide ligand, leading to the formation of a carbamate–palladium complex. More specifically, the reaction step corresponding to the formation of the C–N bond between the amide ligand and the incoming CO_2 was investigated by means of metadynamics simulations (Fig. 10). The model system included the Pd complex and 60 carbon dioxide molecules in a periodically repeating simulation box (supercritical CO_2 conditions were considered). In addition, molecular dynamics simulations in gas phase were also performed.

Comparison of the free energy surface for the process in gas phase and supercritical CO_2 revealed an increase in the free energy barrier for the bulk conditions (6.4 ± 0.5 kcal mol^{-1} in vacuum and 10.7 ± 0.8 kcal mol^{-1} in supercritical CO_2). Analysis of the results for the reverse reaction showed that the change in entropy associated with the dissociation process is less important (increase less) in supercritical CO_2 than in gas phase. This leads to a higher stabilization of the palladium–carbon dioxide complex, pointing out that solvent effects have an important contribution to the stabilization of the palladium–carbon dioxide adduct.

4 Conclusions and Remarks

We have reviewed the application of explicit solvent first-principles molecular dynamics simulation to the study of the reactivity of organometallic systems. We have pointed out how the mechanistic insight provided by this approach may turn

out to be qualitatively and quantitatively different from results of in vacuo and continuum modeling. Indeed, as we have shown, the presence of explicit solvent molecules can have a considerable impact when processes such as proton transfer or the formation of charged or unsaturated species are investigated. This is certainly well established for reactions in water, because of its peculiar properties (high dielectric, hydrogen bonding, acid–base, coordinative), and the early application of the AIMD methodology indeed addressed reactivity in this medium. However, even for nonaqueous solvents, the description of organometallic reactivity may improve when extended systems are considered.

The AIMD methodology is nowadays well established, and in this review, we put the emphasis on its strengths. However, it does also have some limitations. One is certainly the computational cost associated with an increased number of atoms, which limits the time scales that can be investigated. Advanced simulation techniques have been developed in order to promote the occurrence of rare events on the time scale currently accessible (hundreds of ps). Yet, the computational cost remains high, and the exploration of alternative reaction paths or different electronic surfaces remains a challenge. The hybrid quantum mechanical/molecular mechanical approach is an effective way to address larger complexes, especially the ones with bulk ligands that are of high interest for selective transformations.

Having pointed out pros and cons of explicit solvent AIMD simulations applied to organometallic reactivity, it is likely that this approach will continue to coexist and complement the computational chemistry approach based on the potential energy exploration of reduced model systems in the near future. On the long term, however, we would like to push the modeling to the point in which reactants are mixed in a virtual reactor and their transformation to products registered (see, e.g., [139] for a recent report showing that the approach is indeed within our reach). Here, the use of realistic models will certainly be advantageous, as no a priori assumption on which species are relevant for reactivity would be introduced.

Acknowledgments The authors warmly thank all collaborators with whom they share the interest in the application of first-principles simulations to the study of homogeneous catalysis. We specially thank former members of the group Aleix Comas-Vives, Gábor Kovács, and Manuel A. Ortuño and long collaborators as András Stirling, or more recent Nisanth N. Nair, who contributed to some applications presented in this review. The authors thankfully acknowledge the computer resources, technical expertise, and assistance provided by the Barcelona Supercomputing Center (Centro Nacional de Supercomputación). We gratefully acknowledge financial support from Spanish MINECO (CTQ2014-54071-P).

References

1. Cundari TR (ed) (2001) Computational organometallic chemistry. Marcel Dekker, New York
2. Maseras F, Lledós A (eds) (2002) Computational modeling of homogeneous catalysis. Kluwer, Dordrecht
3. Morokuma K, Musaev DG (eds) (2008) Computational modeling for homogeneous and enzymatic catalysis. Wiley, Weinheim

4. Lin Z (2010) Acc Chem Res 43:602
5. Tsang ASK, Sanhueza IA, Schoenebeck F (2014) Chem Eur J 20:1
6. Thiel W (2014) Angew Chem Int Ed 53:2
7. Davidson ER (2000) Chem Rev 100:351
8. Bell AT, Head-Gordon M (2011) Annu Rev Chem Biomol Eng 2:453
9. Cramer CJ, Truhlar DG (1999) Chem Rev 99:2161
10. Tomasi J, Mennucci B, Cammi R (2005) Chem Rev 105:2999
11. Curutchet C, Cramer CJ, Truhlar DG, Ruiz-López MF, Rinaldi D, Orozco M, Luque FJ (2003) J Comput Chem 24:284
12. Sunoj RB, Anand M (2012) Phys Chem Chem Phys 14:12715
13. Ortuño MA, Lledós A, Maseras F, Ujaque G (2014) ChemCatChem 6:3132
14. Diez J, Gimeno J, Lledós A, Suarez FJ, Vicent C (2012) ACS Catal 2:2087
15. Rodríguez-Santiago L, Alí-Torres J, Vidossich P, Sodupe M (2015) Phys Chem Chem Phys 17:13582
16. Van Speybroeck V, Meier RJ (2003) Chem Soc Rev 32:151
17. Margl P, Ziegler T, Blöchl PE (1995) J Am Chem Soc 117:12625
18. De Angelis F, Fantacci S, Sgamellotti A (2006) Coord Chem Rev 250:1497
19. Allen MP, Tildesley DJ (1989) Computer Simulation of Liquids. Oxford University Press, Oxford
20. Frenkel D, Smit B (2001) Understanding molecular simulation: from algorithms to applications. Academic, San Diego
21. Verlet L (1967) Phys Rev 159:98
22. Nose S (1984) Mol Phys 52:255
23. Bussi G, Donadio D, Parrinello M (2007) J Chem Phys 126:014101
24. Martyna GJ, Tobias DJ, Klein ML (1994) J Chem Phys 101:4177
25. Marx D, Hutter J (2009) Ab initio molecular dynamics: basic theory and advanced methods. Cambridge University Press, Cambridge
26. Car R, Parrinello M (1985) Phys Rev Lett 55:2471
27. Hohenberg P, Kohn W (1964) Phys Rev B 136:B864
28. Cramer CJ, Truhlar DG (2009) Phys Chem Chem Phys 11:10757
29. Neese F (2009) Coord Chem Rev 253:526
30. Becke AD (2014) J Chem Phys 140:18A301
31. Kohn W, Sham LJ (1965) Phys Rev 140:1133
32. Parr RG, Yang W (1994) Density-functional theory of atoms and molecules. Oxford University Press, New York
33. Koch W, Holthausen MC (2001) A chemist's guide to density functional theory. Wiley, Weinheim
34. Cohen AJ, Mori-Sanchez P, Yang W (2012) Chem Rev 112:289
35. Zhao Y, Truhlar DG (2008) Theor Chem Acc 120:215
36. Grimme S (2006) J Comput Chem 27:1787
37. Grimme S, Antony J, Ehrlich S, Krieg H (2010) J Chem Phys 132:154104
38. Kulik HJ, Cococcioni M, Scherlis DA, Marzari N (2006) Phys Rev Lett 97:103001
39. VandeVondele J, Sprik MA (2005) Phys Chem Chem Phys 7:1363
40. Marques MAL, Gross EKU (2004) Annu Rev Phys Chem 55:427
41. Neese F (2006) J Biol Inorg Chem 11:702
42. Goedecker S (1999) Rev Mod Phys 71:1085
43. Sulpizi M, Raugei S, VandeVondele J, Carloni P, Sprik M (2007) J Phys Chem B 111:3969
44. Weber V, Bekas C, Laino T, Curioni A, Bertsch A, Futral S (2014) In: Parallel and distributed processing symposium, 2014 IEEE. 28th international 735
45. Warshel A, Levitt M (1976) J Mol Biol 103:227
46. Field MJ, Bash PA, Karplus M (1990) J Comput Chem 11:700
47. Singh UC, Kollman PA (1986) J Comput Chem 7:718
48. Senn HM, Thiel W (2009) Angew Chem Int Ed 48:1198

49. Rovira C (2013) WIREs Comput Mol Sci 3:393
50. Bo C, Maseras F (2008) Dalton Trans 2911
51. Ananikov VP, Musaev DG, Morokuma K (2010) J Mol Catal A Chem 324:104
52. Sameera WMC, Maseras F (2012) WIREs Comput Mol Sci 2:375
53. Woo TK, Margl PM, Deng L, Cavallo L, Ziegler T (1999) Catal Today 50:479
54. Woo TK, Blöchl PE, Ziegler T (2000) J Mol Struct (teochem) 506:313–334
55. Guidoni L, Maurer P, Piana S, Rothlisberger U (2002) Quant Struct-Act Relat 21:119
56. Laino T, Mohamed F, Laio A, Parrinello M (2005) J Chem Theory Comput 1:1176
57. Laino T, Mohamed F, Laio A, Parrinello M (2006) J Chem Theory Comput 2:1370
58. Rowley CN, Roux B (2012) J Chem Theory Comput 8:3526
59. Nielsen SO, Bulo RE, Moore PB, Ensing B (2010) Phys Chem Chem Phys 12:12401
60. Bernstein N, Várnai C, Solt I, Winfield SA, Payne MC, Simon I, Fuxreiter M, Csányi G (2012) Phys Chem Chem Phys 14:646
61. Steinfeld JI, Francisco JF, Hase WL (1998) Chemical kinetics and dynamics. Prentice Hall, Upper Saddle River
62. Pohorille A, Chipot C (eds) (2007) Free Energy Calculations: Theory and Applications in Chemistry and Biology. Springer, Berlin
63. Kirkwood JG (1935) J Chem Phys 3:300
64. Laio A, Parrinello M (2002) Proc Natl Acad Sci U S A 99:12562
65. Barducci A, Bonomi M, Parrinello M (2011) WIREs Comput Mol Sci 1:826
66. Ensing B, De Vivo M, Liu Z, Moore P, Klein ML (2006) Acc Chem Res 39:73
67. Carter EA, Ciccotti G, Hynes JT, Kapral R (1989) Chem Phys Lett 156:472
68. Sprik M, Ciccotti G (1998) J Chem Phys 109:7737
69. Laio A, Gervasio FL (2008) Rep Prog Phys 71:126601
70. Ensing B, Laio A, Parrinello M, Klein ML (2005) J Phys Chem B 109:6676
71. Zheng S, Pfaendtner J (2014) Mol Simul 41:55
72. Laio A, Rodriguez-Fortea A, Gervasio FL, Ceccarelli M, Parrinello M (2005) J Phys Chem B 109:6714
73. Iannuzzi M, Laio A, Parrinello M (2003) Phys Rev Lett 90:238302
74. Bolhuis PG, Chandler D, Dellago C, Geissler PL (2002) Annu Rev Phys Chem 53:291
75. Hutter J, Curioni A (2005) ChemPhysChem 6:1788
76. VandeVondele J, Krack M, Mohamed F, Parrinello M, Chassaing T, Hutter J (2005) Comput Phys Commun 167:103
77. Hassanali AA, Cuny J, Verdolino V, Parrinello M (2014) Phil Trans R Soc A 372:20120482
78. Haber F, Weiss J (1934) Proc R Soc Lond 147:332
79. Bray WC, Gorin MH (1932) J Am Chem Soc 54:2124
80. Ensing B, Buda F, Blöchl PE, Baerends EJ (2001) Angew Chem Int Ed 40:2893
81. Ensing B, Buda F, Blöchl PE, Baerends EJ (2002) Phys Chem Chem Phys 2:3619
82. Yamamoto N, Koga N, Nagaoka M (2012) J Phys Chem B 116:14178
83. Ensing B, Buda F, Gribnau MCM, Baerends EJ (2004) J Am Chem Soc 126:4355
84. Shaik S, Kumar D, de Visser SP, Altun A, Thiel W (2005) Chem Rev 105:2279
85. Louwerse MJ, Vassilev P, Baerends EJ (2008) J Phys Chem A 112:1000
86. Bernasconi L, Baerends EJ (2013) J Am Chem Soc 135:8857
87. Jira R (2009) Angew Chem Int Ed 48:9034
88. Keith JA, Henry PM (2009) Angew Chem Int Ed 48:9038
89. Stirling A, Nair NN, Lledós A, Ujaque G (2014) Chem Soc Rev 43:4940
90. Kovács G, Stirling A, Lledós A, Ujaque G (2012) Chem Eur J 18:5612
91. Nair NN (2011) J Phys Chem B 115:2312
92. Imandi V, Kunnikuruvan S, Nair NN (2013) Chem Eur J 19:4724
93. Bäckvall JE, Akermark B, Ljunggren SO (1979) J Am Chem Soc 101:2411
94. Beyramabadi SA, Eshtiagh-Hosseini H, Housaindokht MR, Morsali A (2009) J Mol Struct (THEOCHEM) 903:108
95. Henry PM (1973) J Org Chem 38:2415

96. Heck RF (1968) Hercules Chem 57:12
97. Keith JA, Nielsen RJ, Oxgaard J, Goddard WA (2006) J Am Chem Soc 128:3132
98. Imandi V, Nair NN (2015) J Phys Chem B 119:11176
99. Carloni P, Sprik M, Andreoni W (2000) J Phys Chem B 104:823
100. Bose RN, Cornelius RD, Viola RE (1984) J Am Chem Soc 106:3336
101. Lau JKC, Ensing B (2010) Phys Chem Chem Phys 12:10348
102. Melchior A, Tolazzi M, Martínez JM, Pappalardo RR, Sánchez-Marcos E (2015) J Chem Theory Comput 11:1735
103. Noyori R, Hashiguchi S (1997) Acc Chem Res 30:97
104. Pavlova A, Meijer EJ (2012) ChemPhysChem 13:3492
105. Bandaru S, English NJ, MacElroy JMD (2014) J Comput Chem 35:683
106. Li P, Henkelman G, Keith JA, Johnson JK (2014) J Phys Chem C 118:21385
107. Lewis NS, Nocera DG (2008) Proc Natl Acad Sci U S A 103:15729
108. Kohl SW, Winer L, Schwartsburd L, Konstantinovski L, Shimon LJW, Ben-David Y, Iron MA, Milstein D (2009) Science 324:74
109. Ma C, Piccinin S, Fabris S (2012) ACS Catal 2:1500
110. Vallés-Pardo JL, Guijt MC, Iannuzzi M, Joya KS, de Groot HJM, Buda F (2012) ChemPhysChem 13:140
111. Vallés-Pardo JL, de Groot HJM, Buda F (2012) Phys Chem Chem Phys 14:15502.
112. Shilov AE, Shul'pin GB (1997) Chem Rev 97:2879
113. Vidossich P, Ujaque G, Lledos A (2012) Chem Commun 48:1979
114. Bühl M, Golubnychiy V (2007) Organometallics 26:6218
115. Bühl M, Wipff G (2011) ChemPhysChem 12:3095
116. Bühl M, Kabrede H (2006) Inorg Chem 45:3834
117. Bühl M, Schreckenbach G (2010) Inorg Chem 49:3821
118. Shamov GA, Schreckenbach G (2008) J Am Chem Soc 130:13735
119. Szabo Z, Grenthe I (2007) Inorg Chem 46:9372
120. Rodríguez-Fortea A, Vilà-Nadal L, Poblet JM (2008) Inorg Chem 47:7745
121. Vilà-Nadal L, Rodríguez-Fortea A, Poblet JM (2009) Eur J Inorg Chem 5125
122. Jiménez-Lozano P, Carbó JJ, Chaumont A, Poblet JM, Rodríguez-Fortea A, Wipff G (2014) Inorg Chem 53:778
123. Moret ME, Tavernelli I, Rothlisberger U (2009) J Phys Chem B 113:7737
124. Moret ME, Tavernelli I, Chergui M, Rothlisberger U (2010) Chem Eur J 16:5889
125. Daku LML, Hauser A (2010) J Phys Chem Lett 1:1830
126. Truflandier LA, Autschbach J (2010) J Am Chem Soc 132:3472
127. Beret EC, Pappalardo RR, Doltsinis NL, Marx D, Sánchez-Marcos E (2008) ChemPhysChem 9:237
128. Beret EC, Martínez JM, Pappalardo RR, Sánchez-Marcos E, Doltsinis NL, Marx D (2008) J Chem Theory Comput 4:2108
129. Vidossich P, Ortuño M, Ujaque G, Lledós A (2011) ChemPhysChem 12:1666
130. Zahn S, Brehm M, Brüssel M, Hollóczki O, Kohagen M, Lehmann S, Malberg F, Pensado AS, Schöppke M, Weber H, Kirchner B (2014) J Mol Liq 192:71
131. Pu M, Privalov T (2015) Isr J Chem 55:179
132. Dub PA, Henson NJ, Martin RL, Gordon JC (2014) J Am Chem Soc 136:3505
133. Handgraaf JW, Meijer EJ (2007) J Am Chem Soc 129:3099
134. Vidossich P, Ujaque G, Lledós A (2014) Chem Commun 50:661
135. Ortuño MA, Vidossich P, Ujaque G, Conejero S, Lledós A (2013) Dalton Trans 42:12165
136. Rowley CN, Woo TK (2010) Organometallics 30:2071
137. Aresta M (2010) Carbon dioxide as chemical feedstock. Wiley, Weinheim
138. Brüssel M, di Dio PJ, Muñiz K, Kirchner B (2011) Int J Mol Sci 12:1389
139. Wang LP, Titov A, McGibbon R, Liu F, Pande VS, Martínez TJ (2014) Nat Chem 6:1044